Multilamellar nanovesicles show distinct mechanical properties depending on their degree of lamellarity

Nanoscale

PAPER

View Article Online
View Journal | View Issue

Cite this: *Nanoscale*, 2018, **10**, 5318

Multilamellar nanovesicles show distinct mechanical properties depending on their degree of lamellarity†

Daan Vorselen,[a,b] Margherita Marchetti,[a] Carmen López-Iglesias,[c] Peter J. Peters,[c] Wouter H. Roos*‡[a,d] and Gijs J. L. Wuite*‡[a]

Received 12th December 2017,
Accepted 23rd February 2018

DOI: 10.1039/c7nr09224e

rsc.li/nanoscale

Small multilamellar vesicles may have benefits over unilamellar vesicles for drug delivery, such as an increased volume for hydrophobic drugs. In addition, their altered mechanical properties might be beneficial for cellular uptake. Here, we show how atomic force microscopy (AFM) can be used to detect and characterize multilamellar vesicles. We quantify the size of each break event occurring during AFM nanoindentations, which shows good agreement with the thickness of supported lipid bilayers. Analyzing the size and number of these events for individual vesicles allows us to distinguish between vesicles consisting of 1 up to 5 bilayers. We validate these results by comparison with correlative cryo-electron microscopy (cryo-EM) data at the vesicle population level. Finally, we quantify the vesicle geometry and mechanical properties, and show that with additional bilayers adherent vesicles are more spherical and stiffer. Surprisingly, at ~20% stiffening for each additional bilayer, the vesicle stiffness scales only weakly with lamellarity. Our results show the potential of AFM for studying liposomal nanoparticles and suggest that small multilamellar vesicles may have beneficial mechanical properties for cellular uptake.

Introduction

Nanovesicles are currently used as nanocarriers in drug delivery, for example for cancer therapeutics[1,2] and treatment of protozoan infections.[2,3] Characteristic properties of these vesicles can be tuned by changing their degree of lamellarity, and it has been suggested that small multilamellar vesicles (SMVs: ~100 nm) can have important benefits over small unilamellar vesicles (SUVs: ~100 nm). For instance, many drugs are hydrophobic[4] and SMVs have more volume for encapsulation of hydrophobic molecules than similar sized SUVs. SMVs also result in slower release kinetics, and antigen carrying SMVs have furthermore been shown to form a much more potent vaccine than SUVs.[5] SMVs with cross-linked lipid bilayers seem to have enhanced therapeutic benefits.[5,6] On the other hand, multilamellarity also occurs as an uncontrolled side effect when trying to achieve a high loading rate of water soluble molecules into vesicles; the high concentration of vesicles, which is used to achieve efficient loading, results in formation of multilamellar vesicles.

The mechanical properties of vesicles, and more generally of nanoparticles, is potentially an important factor for interaction with cells and hence for drug delivery.[7,8] It has been shown that increasing the rigidity of particles, and vesicles specifically, significantly facilitated their uptake by cells.[9–11] These results are supported by theoretical models which suggest that stiffer particles stay in a more spherical shape upon binding to a cell membrane, leading to more efficient cellular uptake.[12,13] Furthermore, it was reported that the mechanical properties of nanoparticles can influence the uptake mechanism,[14] as well as circulation and targeting.[15] These results show the relevance of vesicle mechanics for drug delivery. Notably, multilamellarity could have a strong influence on the mechanical properties of vesicles and therefore potentially on cellular uptake. However, a quantification of the impact of the degree of multilamellarity on the mechanical properties is currently lacking.

In this study, we quantify the mechanics of SMVs using atomic force microscopy (AFM). AFM nanoindentation is a proven technique to study the material properties of nano-

[a]*Department of Physics and Astronomy and LaserLab, Vrije Universiteit, Amsterdam, 1081 HV, The Netherlands. E-mail: g.j.l.wuite@vu.nl*
[b]*Department of Oral Function and Restorative Dentistry, Academic Centre for Dentistry Amsterdam (ACTA), Research Institute MOVE, University of Amsterdam and Vrije Universiteit, Amsterdam, 1081LA, The Netherlands*
[c]*The Maastricht Multimodal Molecular Imaging Institute (M4I), Maastricht University, Netherlands*
[d]*Moleculaire Biofysica, Zernike Instituut, Rijksuniversiteit Groningen, Nijenborgh 4, 9747 AG Groningen, the Netherlands. E-mail: w.h.roos@rug.nl*
†Electronic supplementary information (ESI) available. See DOI: 10.1039/c7nr09224e
‡These authors contributed equally.

particles, such as viruses,[16–18] liposomes[19,20] and natural vesicles.[21–23] Recently, we applied AFM to study the mechanics of small unilamellar vesicles and introduced a new quantitative model based on Canham–Helfrich theory[24,25] to describe their mechanical response.[20] AFM has also been used to study the penetration, or equivalently puncturing, of supported lipid bilayers.[26–28] However, it remains challenging to characterize individual breaks events during nanoindentation of fluid bilayer stacks.[29] In this work, however, we show that by performing AFM nanoindentations we can determine the degree of lamellarity for individual vesicles by analyzing bilayer penetrations. The distribution of lamellarities present in the vesicle populations corresponds well to cryoEM data. This allows us to study the physical differences between vesicles with 1 up to 5 bilayers. We find that SMVs stay in a more spherical shape upon adhesion with a surface. SMVs are also stiffer than SUVs, however, the stiffness of adherent vesicles is only weakly dependent on the degree of lamellarity. These properties are potentially beneficial for drug delivery.

Results and discussion

Recently, we described the mechanics of unilamellar nanovesicles.[20] In the current work, we applied a vesicle preparation protocol, which, using a higher concentration of lipids and leaving out freeze–thaw cycles, gives rise to a high percentage of multilamellar vesicles. The vesicles were made of a complex lipid mixture and extruded through 200 nm filters (see Experimental section). Subsequently they were attached to 0.001% poly-L-lysine coated glass surfaces. For the mechanical probing of the vesicles, first, an image of individual particles was recorded. Subsequently, we performed nanoindentation experiments to obtain force deformation curves (FDCs).[16] Initially, an indentation was made until a maximum force of 0.5 nN. These low-force indentations show strong overlap between approach and retract curves, showing that the observed behavior is elastic (Fig. 1). This first indentation was followed by at least one more indentation until a maximum force of 10 nN (Fig. 1). For high-force indentations we sometimes observe similar behavior as previously predicted and described for SUVs:[20] the FDC first shows an approximately linear force response, which is followed by a flattening of the curve, corresponding to inward lipid tether formation. Next, there is a steep rise in force, supposedly due to the two lipid bilayers being pressed together. Finally, two discontinuities are visible, which likely corresponds to the penetration of the two lipid bilayers. Thereafter, the AFM tip touches the glass surface (Fig. 1A and inset), which appears infinitely rigid. However, for different vesicles more discontinuities occurred close to the glass surface, which suggests that more lipid bilayers are penetrated and hence that these vesicles are multilamellar (Fig. 1B and C). Interestingly, vesicle indentations also reveal discontinuities further from the glass (Fig. 1C and D), which calls for a systematic analysis of these discontinuities to determine lamellarity.

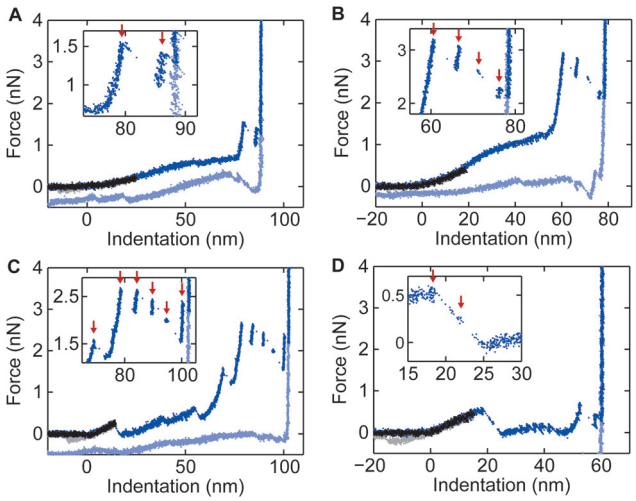

Fig. 1 Typical force indentation curves on unilamellar and multilamellar nanovesicles. First a low-force indentation was performed (black = approach, grey = retract). The approach and retract curves highly overlap (the retract curve is mostly behind the approach curve and therefore hard to see in panel A & B), indicating elastic behavior. In dark blue, a subsequent indentation until a 10 nN max. force (retract in light blue, negative forces indicate vesicle-AFM tip adhesion). Force is initially zero till the contact point (at indentation 0 nm), then a subsequent rise in force follows. Finally, multiple breaks events can be observed close to the surface, which is visible as a nearly vertical response. Vesicles showing (A) 2, (B) 4 and (C) 6 break events close to the surface (magnified and identified with arrows in insets). The last break closest to the surface is visibly smaller than the other breaks. (C, D) Breaks can also occur far from the surface. These breaks occur in similar sized steps (~4 nm) (D, inset).

In total, we recorded 561 break events in FDCs made on 124 vesicles. To examine these events, we separated out discontinuities occurring close to the glass surface, *i.e.* those occurring within ~3 nm from the surface or from a subsequent discontinuity (*e.g.* the discontinuities in the insets of figure panels 1A–C). Such breaks typically occur after a steep rise in force when presumably the bilayers are compressed into a stack. We quantified the distance of the discontinuities, which shows a bimodal distribution with peaks at 2.00 ± 0.05 nm and 4.98 ± 0.07 nm (s.e.m. (standard error of the mean), N = 361) (Fig. 2A) for the discontinuities close to the surface. The 5 nm peak corresponds to previously reported bilayer thicknesses.[30,31] The 2 nm peak is caused almost exclusively by the last discontinuity before the glass surface, which are 1.94 ± 0.04 nm (s.e.m., 114 events with break size <4 nm, from 124 in total) (Fig. 2A). We separately investigated the breaks occurring further from the surface (N = 200). Unlike nanoparticles that behave like thin elastic shells (*e.g.* some viruses), which buckle during nanoindentations,[32,33] no such discontinuity is expected during indentations of vesicles with fluid membranes.[20] These breaks could therefore correspond to bilayer penetration events. The vesicle indentations suggest that these discontinuities can occur in steps of a specific size (Fig. 1D, inset). Indeed, we observe a large peak around a break size of 4.0 ± 0.1 nm (s.e.m., N = 159) (Fig. 2B), again corresponding to

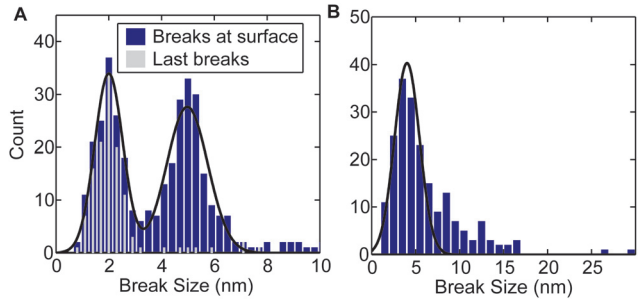

Fig. 2 Analysis of breaks occurring in FDCs on vesicles. (A) In blue, histogram of breaks occurring close to the surface (N = 361 breaks in indentations on 124 vesicles, 15 breaks showed a break size above 10 nm and are not shown). In grey, histogram of the final break occurring before reaching the surface (N = 124). In black a bimodal Gaussian fit of breaks <7 nm, with peaks at 2.00 ± 0.05 nm and 4.98 ± 0.07 nm (s.e.m.). (B) Breaks occurring farther from the surface (>3 nm from the surface or a subsequent break, *e.g.* the discontinuities in the inset of figure panel 1D) in blue (N = 200). In black a Gaussian fit of breaks <7 nm (N = 159) with peak at 4.0 ± 0.1 nm (s.e.m.). Some of the larger breaks (>7 nm) could correspond to penetration of multiple bilayers at once.

reported bilayer thicknesses[30,31] and therefore suggesting that these breaks could also correspond to bilayer penetrations. Interestingly, the break events further from the surface occurred at significantly lower forces (~1 nN) than the bilayer penetrations close to the surface (~2 nN). This could be related to differences in loading rate[34] (Fig. S1†).

The thickness of lipid bilayers is typically in the range 3–5 nm,[30,31] however, we wanted to compare the break sizes found during vesicle indentations with the thickness of lipid bilayers with identical lipid composition. For this purpose, AFM imaging can be used to rupture vesicles, resulting in supported lipid bilayers;[35] in our experiments we induced vesicle rupture by imaging with a high force (~2 nN). By subsequent AFM imaging at low force (Fig. 3A) we found that the thickness of our lipid bilayers is 4.1 ± 0.2 nm (s.e.m., N = 4) (Fig. 3B). Note that for this estimate of the bilayer height we compress the bilayer somewhat due to the imaging force (~100 pN). By performing nanoindentations on these lipid bilayers we measured the thickness by quantifying the distance from the contact point till the surface which should give a better estimate of the thickness, resulting in 5.2 ± 0.2 nm (s.e.m., N = 54) (Fig. 3C), which indeed corresponds well to the size of the larger breaks occurring close to the surface. The force required for penetrating supported lipid bilayers exceeds the force observed during vesicle indentation, which may be related to the membrane tension present in the adherent vesicles[36] (Fig. S1†). During indentations, we observed that our bilayers deformed strongly and continuously (3.6 nm ± 0.2 nm) before they show a small break (1.78 ± 0.05 nm, s.e.m., N = 54). The size of these breaks corresponds well to the final breaks before reaching the surface in vesicle indentations. This suggests that a ~2 nm break occurs when puncturing a deformed bilayer on a stiff surface, because the jump is between a highly deformed state of the bilayer and the solid surface underneath. The 4–5 nm breaks of the indented vesicles on the other hand are then a result of penetrating a deformed bilayer on top of another deformable bilayer. This suggests that the vast majority of the observed break events in the nanoindentations experiments on vesicles correspond to bilayer penetrations.

Next, we summed the distance of all breaks for each vesicle indentation curve (Fig. 4A). We observed a broad distribution of this total distance, with multiple peaks. To find the location of the peaks we fitted a mixture of five Gaussian distributions, revealing peaks at 7.3 ± 0.3, 15.9 ± 0.9, 22.9 ± 1.1, 29.4 ± 1.8 and 40.8 ± 1.6 nm (s.e.m. determined by bootstrapping). These values correspond well to multiples of 8 nm, which is approxi-

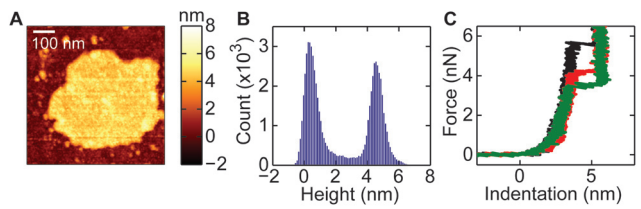

Fig. 3 Imaging and indentation of supported lipid bilayers. (A) Typical supported lipid bilayer created by AFM scanning of vesicles at a high force (~2 nN). Image recorded at peak imaging forces of ~100 pN. (B) Histogram of the height of each pixel of image 3A. The height of the bilayer was determined as the distance between the peaks (4.1 ± 0.2 nm (s.e.m.), N = 4 bilayers). (C) Typical FDCs performed on solid supported lipid bilayers. Different colors mark indentations at different locations.

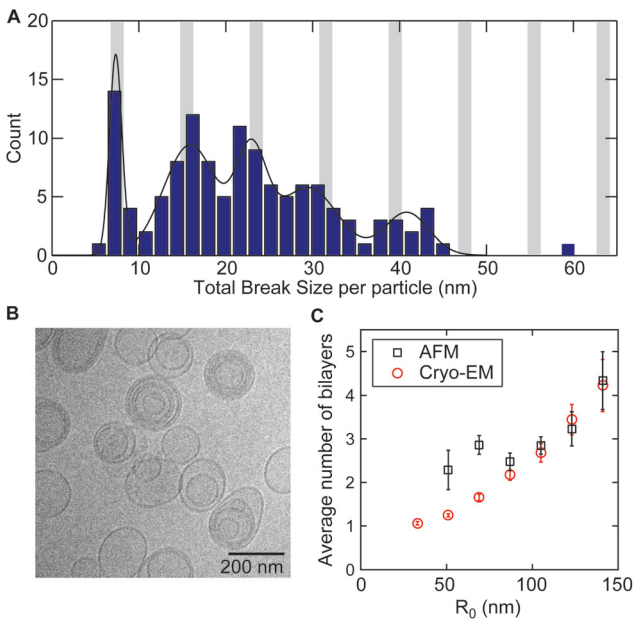

Fig. 4 Determination of the vesicle degree of lamellarity. (A) Total break distance summed per vesicle (N = 124). In black a multimodal Gaussian fit (5 components, with peaks at 7.3 ± 0.3, 15.9 ± 0.9, 22.9 ± 1.1, 29.4 ± 1.8 and 40.8 ± 1.6 nm (s.e.m.)). In light grey the expected total break distance for vesicles with 1,2, ..., 8 bilayers, assuming a bilayer thickness of 8 nm. (B) Cryo-EM image of the vesicles. (C) Average number of lipid bilayers for vesicles as function of the radius.

mately two times the height of a lipid bilayer. This indicates that we indented vesicles with 1 to 5 lipid bilayers and that we can distinguish vesicles based on their number of bilayers. For further analysis, we separated the vesicles by their lamellarity based on binning between the minima in the multimodal Gaussian fit (Fig. S2†).

To establish how well we can determine the lamellarity of vesicles using AFM, we used CryoEM for an independent measure of the distribution of degree of lamellarity for the vesicle population. We determined the lamellarity of vesicles by CryoEM images revealed a distribution of vesicle lamellarities present in the vesicle population (Fig. 4B). Since the degree of lamellarity depends on the vesicle size, we compared the AFM and CryoEM data by the average number of bilayers for different vesicle sizes (Fig. 4C). Especially for the larger vesicles, the two measurements correspond very well. The deviation for smaller vesicles could be partially caused by our preference for higher vesicles in the AFM experiments. Overall, the good correspondence of these data indicates that we can indeed detect the number of bilayers accurately using AFM nanoindentation. This encouraged us to look into the effect of number of bilayers on the physical properties of vesicles.

First, we examined the shape of the vesicles adhering to the surface. Adherent vesicles typically deform on the surface,[20,37] where the optimal shape is that of a spherical cap, in which the degree of spreading is a balance of bending and stretching of the bilayer, adhesion energy to the surface and a build-up of internal osmotic pressure.[38] We obtained quantitative information on the shape of individual vesicles by creating a line profile along the slow scanning axes through the maximum height H of a vesicle. We determined the radius of curvature R_c by fitting a circular arc to the part of the line profile above half of the maximum height. We then quantified the shape of the vesicle by dividing the height by the radius of curvature (Fig. 5A and inset). This value is 2 for a sphere and 1 for a hemisphere. We corrected these measures for tip convolution and deformation during imaging (see Experimental section). Most vesicles formed spherical caps with H/R_c between 0.7 and 1. We observed a clear increase of this ratio with increasing degree of lamellarity, showing that multilamellar vesicles spread less and stay in a more spherical shape upon adhesion (Fig. 5A).

Since the external chemical properties for unilamellar and multilamellar vesicles are identical, their adhesion energy to the surface is identical too. Hence, the more spherical shape suggests that the multilamellar vesicles are stiffer. To test this more directly we measured the vesicle stiffness (*i.e.* spring constant) using the initial slope of the indentation curve (measured between indentation of 0.02–0.1 R_c or until the first discontinuity if it occurred at smaller indentation). We observed a clear increase, which appears strikingly linear, in stiffness with each added bilayer, from 0.015 ± 0.002 N m^{-1} (s.e.m., N = 26) for unilamellar vesicles to 0.027 ± 0.002 N m^{-1} (s.e.m., N = 14) for vesicles with 5 lipid bilayers (Fig. 5B). Fitting a linear relation to this data revealed a slope of 0.0027 N m^{-1} per added bilayer. This corresponds to an increase of only ~20% of the stiffness of an unilamellar vesicle with each added layer.

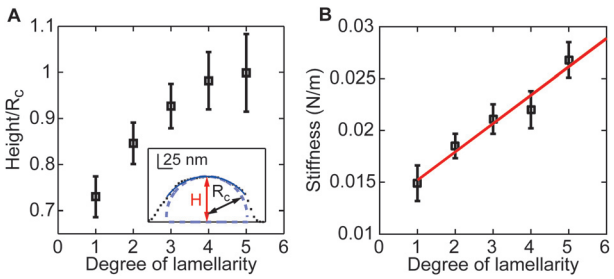

Fig. 5 Effect of multilamellarity on vesicle geometry and mechanics. (A) Shape of vesicles as quantified by the height divided by radius of curvature (R_c). Adherent vesicles containing more bilayers are less flattened. Inset shows how vesicle shape was quantified. Line profile as measured by AFM in dotted black. In dark blue the fitted circular arc and in light blue the cap shape after tip correction (see Experimental section). Height and radius of curvature are marked with arrows. (B) Stiffness (spring constant) of vesicles (measured between 0.02 and 0.1 R_c). Vesicles with more lipid bilayers are stiffer. In red a linear fit. Slope corresponds to ~2.7 × 10^{-3} N m^{-1} per bilayer. Errorbars in both panels correspond to s.e.m.

Discussion and conclusion

In this work, we identified multilamellar vesicles by quantifying the total size of the break events occurring during nanoindentations (Fig. 1 and 4A). These penetration events have been previously observed in studies on solid supported bilayers[26] and during vesicle indentations.[19] It was also previously observed that when indenting multiple fluid bilayers, the break closest to the surface is smaller.[28,39] Our data on supported fluid lipid bilayers indeed suggests that they are strongly deformed, to less than half of their initial thickness, before they are penetrated (Fig. 3C). Although this has been observed previously,[34] the processes that lead to this extent of deformation are unknown. Strong deformation is presumably due to tilting of phospholipid molecules and bending of their hydrocarbon chains, and perhaps interdigitation of the two leaflets.

We see a clear effect of the amount of lipid bilayers on the vesicle stiffness (Fig. 5B). Our data can be well described by a linear relation with 2.7 × 10^{-3} N m^{-1} stiffness added per lipid bilayer. Typically, the mechanics of fluid lipid vesicles are described in terms of two intrinsic material properties, *i.e.* a bending modulus κ and a stretch modulus σ.[20,24,25,40,41] Since the applied force by the AFM tip is perpendicular to the bilayer plane, the contribution of stretching is expected to be negligible. In case of bending alone, a SMV could be approximated by parallel springs and an increase of ~100% in stiffness would be expected for each internal vesicle. Hence, the ~20% added stiffness per additional bilayer observed here seems inconsistent with bending alone. In previous work we reported that the high stiffness of adherent unilamellar vesicles, too, is

inconsistent with bending alone (in which case the vesicle stiffness is expected to be $\sim 28\kappa R_c^{-2} \approx 10^{-4}$ Nm^{-1}) and can instead be described more accurately using an additional term corresponding to an osmotic pressure difference over the membrane ($\Pi_{internal} > \Pi_{external}$), which builds up during vesicle spreading onto the surface and leads to vesicle stiffening.[20] Qualitatively, such pressurization is consistent with the results presented here. Due to the development of osmotic pressure in the outermost vesicle during spreading onto the surface,[38] internal vesicles are expected to deform in a balance of bending and osmotic pressure themselves. In equilibrium this will result in an osmotic pressure ($\Pi_{external} > \Pi_{internal}$) over the internal membrane. This pressure difference is likely small compared to the pressure difference over the outermost membrane since it is not driven by adhesion to the surface, and balanced by membrane bending alone. Therefore, the presence of an internal vesicle is expected to lead to a modest increase in pressure difference over the outermost membrane ($\Pi_{internal} > \Pi_{external}$) and similar modest increase in vesicle stiffness. Moreover, when the internal membranes are less pressurized than the outer membrane, they will also resist deformation during AFM indentation less strongly.

Conclusion

In summary, our study shows that we can detect and measure mechanical properties of multilamellar vesicles by AFM nanoindentations. The observed response is in agreement with our recently proposed model, which described vesicles indentation using Canham–Helfrich theory.[20] SMVs stay in a more spherical shape and are stiffer than SUVs. These properties were previously shown to be beneficial for cellular uptake.[9,10,12,13] According to these findings, our results suggest that the degree of lamellarity of small vesicles can be tuned for beneficial physical properties for drug delivery.

Experimental section

Vesicle preparation

EggPC (P2772) and Cholesterol (C8667) were ordered from Sigma. Brain PS (840032C) was ordered from Avanti Polar lipids. Egg PE and Egg SM were ordered from Lipoid. Small MLVs were produced using the extrusion method.[42] In short: lipid powder was dissolved at 20 mg mL^{-1} in a 9 : 1 $CHCL_3$: CH_3OH solution in a round bottom flask. Molar ratio of mixed lipids was 15% Egg PC, 17% Egg PE, 8% Brain PS, 15% Egg SM and 45% cholesterol. This complex lipid mixture is designed to mimic the lipid concentrations in the red blood cell[43] and similarly vesicles excreted by red blood cells.[44] The solvent was dried in a rotary evaporator (Buchi), first for 1 hour at 400 mBar, then subsequently at least another 30 minutes at 100 mBar. Vesicles with equal buffer conditions in the lumen and on the outside were created by dissolving the dried lipids in PBS (Phosphate buffered saline: 10 mM phosphate, 150 mM sodium chloride, pH 7.3–7.5) (Invitrogen) at a 20 mg ml^{-1} final concentration. Vesicles were then vortexed for 10 minutes. Finally, vesicles were extruded 15 times back and forth through a 200 nm filter (Avanti polar lipids).

AFM

Vesicles were adhered to poly-L-lysine coated glass slides in PBS. Slides were first cleaned in a 96% ethanol, 3% HCl solution for 10 minutes. Afterwards they were coated for 1 hour in a 0.001% poly-L-lysine solution (Sigma), rinsed with ultrapure water and dried overnight at 37 °C. They were stored at 7 °C for a maximum of 1 month. A 50 μL droplet of vesicle solution was incubated on the glass slide. Vesicles were imaged in PeakForce Tapping™ Mode on a Bruker Biocatalyst setup. Force setpoint during imaging was 100 pN. Nanoindentations were performed by first making an image of a single particle, indenting it at 0.5 nN, and subsequently 10 nN with a speed of 250 nm s^{-1}. Subsequently another image was made to check for movement of the vesicle. Importantly, both before and after the vesicle indentation, the tip was checked for adherent lipid bilayers by pushing on the glass surface till a force of 5 nN. Tips used were silicon nitride tips with a nominal tip radius of 15 nm on a 0.1 N m^{-1} cantilever by Olympus (OMCL-RC800PSA). Individual cantilevers were calibrated using thermal tuning.

AFM image analysis

Both images and force curves were processed using home-built MATLAB software. Size and shape of vesicles were analyzed as described previously.[20] Briefly, a circular arc was fit to the part of the vesicle above half of the maximum height. Subsequently the tip size was subtracted. Height of the vesicles was determined from the FDC. Radius of curvature was corrected by 2.5 times the height found in the FDC minus the height found in the images. Size of the vesicle before deformation was calculated assuming surface area conservation. A minimum radius of curvature of 5 nm was assumed for where the spherical cap touches the surface.

AFM FDC analysis

The cantilever response was measured on the sample surface and fitted linearly. The resulting fit was subtracted from the measured response when indenting vesicles to obtain FDCs. The stiffness (or spring constant) of the vesicles was found by fitting the FDC with a straight line in the interval between 0.02–0.1 R_c (a single FDC per vesicle was used). For assigning lamellarity to the vesicles, they were binned between the minima of the multi-modal gaussian fit in Fig. 4.

Cryo-EM

For the cryo-preparation, glow-discharged R2/2200 mesh holey carbon films (Quantifoil) were used. 2.5 μL of sample was applied to the grid and blotted for 2.5 s and then cryo-plunged using a Vitrobot (Thermo Fisher Scientific, The Netherlands). In total 90 micrographs were collected on a Tecnai Spirit (120 kV) cryo-electron microscope using a Eagle 4k × 4k CCD

camera (Thermo Fisher Scientific). CryoEM images were analyzed by measuring the circumference of individual vesicles and counting the amount of lipid bilayers. A small percentage of multivesicular vesicles was present, in which case only the bilayers of the internal vesicle with the highest degree of lamellarity were counted.

Conflicts of interest

There are no conflicts to declare.

Acknowledgements

The authors thank L. Dreesens for helpful discussions and help collecting preliminary data and Hans Duimel for helping in the cryoEM sample preparation. WHR and GJLW acknowledge funding *via* respectively a Nederlandse Wetenschappelijke Organisatie (NWO) VIDI and VICI grant and funding *via* FOM projectruimte grants. DV, WHR and GJLW acknowledge the Dutch Space Organization (SRON, grant MG-10-07).

References

1 A. Z. Wang, R. Langer and O. C. Farokhzad, *Annu. Rev. Med.*, 2012, **63**, 185–198.
2 V. P. Torchilin, *Nat. Rev. Drug Discovery*, 2005, **4**, 145–160.
3 M. Balasegaram, K. Ritmeijer, M. A. Lima, S. Burza, G. Ortiz Genovese, B. Milani, S. Gaspani, J. Potet and F. Chappuis, *Expert Opin. Emerging Drugs*, 2012, **17**, 493–510.
4 C. Wischke and S. P. Schwendeman, *Int. J. Pharm.*, 2008, **364**, 298–327.
5 J. J. Moon, H. Suh, A. Bershteyn, M. T. Stephan, H. Liu, B. Huang, M. Sohail, S. Luo, S. H. Um, H. Khant, J. T. Goodwin, J. Ramos, W. Chiu and D. J. Irvine, *Nat. Mater.*, 2011, **10**, 243–251.
6 K. Il Joo, L. Xiao, S. Liu, Y. Liu, C. L. Lee, P. S. Conti, M. K. Wong, Z. Li and P. Wang, *Biomaterials*, 2013, **34**, 3098–3109.
7 I. Canton and G. Battaglia, *Chem. Soc. Rev.*, 2012, **41**, 2718.
8 H. Ding and Y. Ma, *Small*, 2015, **11**, 1055–1071.
9 L. Zhang, Q. Feng, J. Wang, S. Zhang, B. Ding, Y. Wei, M. Dong, J. Ryu, T. Yoon, X. Shi, J. Sun and X. Jiang, *ACS Nano*, 2015, **9**, 9912–9921.
10 J. Sun, L. Zhang, J. Wang, Q. Feng, D. Liu, Q. Yin, D. Xu, Y. Wei, B. Ding, X. Shi and X. Jiang, *Adv. Mater.*, 2015, **27**, 1402–1407.
11 N. Kol, M. Gladnikoff, D. Barlam, R. Z. Shneck, A. Rein and I. Rousso, *Biophys. J.*, 2006, **91**, 767–774.
12 X. Yi, X. Shi and H. Gao, *Phys. Rev. Lett.*, 2011, **107**, 98101.
13 X. Yi and H. Gao, *Soft Matter*, 2015, **11**, 1107–1115.
14 X. Banquy, F. Suarez, A. Argaw, J.-M. Rabanel, P. Grutter, J.-F. Bouchard, P. Hildgen and S. Giasson, *Soft Matter*, 2009, **5**, 3984.
15 A. C. Anselmo, M. Zhang, S. Kumar, D. R. Vogus, S. Menegatti, M. E. Helgeson and S. Mitragotri, *ACS Nano*, 2015, **9**, 3169–3177.
16 W. H. Roos, R. Bruinsma and G. J. L. Wuite, *Nat. Phys.*, 2010, **6**, 733–743.
17 M. Marchetti, G. Wuite and W. Roos, *Curr. Opin. Virol.*, 2016, **18**, 82–88.
18 P. J. de Pablo and M. G. Mateu, in *Structure and Physics of Viruses*, 2013, pp. 519–551.
19 S. Li, F. Eghiaian, C. Sieben, A. Herrmann and I. A. T. Schaap, *Biophys. J.*, 2011, **100**, 637–645.
20 D. Vorselen, F. C. MacKintosh, W. H. Roos and G. J. L. Wuite, *ACS Nano*, 2017, **11**, 2628–2636.
21 A. Calò, D. Reguera, G. Oncins, M.-A. Persuy, G. Sanz, S. Lobasso, A. Corcelli, E. Pajot-Augy and G. Gomila, *Nanoscale*, 2014, **6**, 2275–2285.
22 D. Vorselen, S. M. van Dommelen, R. Sorkin, J. Schiller, R. van Wijk, R. M. Schiffelers, G. J. L. Wuite and W. H. Roos, *bioRxiv*, 2017, 212456.
23 S. Sharma, H. I. Rasool, V. Palanisamy, C. Mathisen, M. Schmidt, D. T. Wong and J. K. Gimzewski, *ACS Nano*, 2010, **4**, 1921–1926.
24 W. Helfrich, *Z. Naturforsch., C: J. Biosci.*, 1973, **28**, 693–703.
25 P. B. Canham, *J. Theor. Biol.*, 1970, **26**, 61–81.
26 S. Garcia-Manyes and F. Sanz, *Biochim. Biophys. Acta, Biomembr.*, 2010, **1798**, 741–749.
27 Y. F. Dufrêne, T. Boland, J. W. Schneider, W. R. Barger and G. U. Lee, *Faraday Discuss.*, 1998, 79–94.
28 V. Franz, S. Loi, H. Müller, E. Bamberg and H. J. Butt, *Colloids Surf., B*, 2002, **23**, 191–200.
29 L. Redondo-Morata, M. I. Giannotti and F. Sanz, *Langmuir*, 2012, **28**, 6403–6410.
30 W. Rawicz, K. C. Olbrich, T. Mcintosh, D. Needham and E. Evans, *Biophys. J.*, 2000, **79**, 328–339.
31 T. J. McIntosh, S. a. Simon, D. Needham and C. H. Huang, *Biochemistry*, 1992, **31**, 2012–2020.
32 W. S. Klug, R. F. Bruinsma, J.-P. Michel, C. M. Knobler, I. L. Ivanovska, C. F. Schmidt and G. J. L. Wuite, *Phys. Rev. Lett.*, 2006, **97**, 228101.
33 W. H. Roos, K. Radtke, E. Kniesmeijer, H. Geertsema, B. Sodeik and G. J. L. Wuite, *Proc. Natl. Acad. Sci. U. S. A.*, 2009, **106**, 9673–9678.
34 A. Alessandrini, H. M. Seeger, T. Caramaschi and P. Facci, *Biophys. J.*, 2012, **103**, 38–47.
35 R. P. Richter and A. R. Brisson, *Biophys. J.*, 2005, **88**, 3422–3433.
36 A. J. García-Sáez, S. Chiantia, J. Salgado and P. Schwille, *Biophys. J.*, 2007, **93**, 103–112.
37 D. L. M. Rupert, G. V. Shelke, G. Emilsson, V. Claudio, S. Block, C. Lässer, A. Dahlin, J. O. Lötvall, M. Bally, V. P. Zhdanov and F. Höök, *Anal. Chem.*, 2016, **88**, 9980–9988.
38 U. Seifert and R. Lipowsky, *Phys. Rev. A*, 1990, **42**, 4768–4771.

39 I. Pera, R. Stark, M. Kappl, H.-J. Butt and F. Benfenati, *Biophys. J.*, 2004, **87**, 2446–2455.
40 P. Bassereau, B. Sorre and A. Lévy, *Adv. Colloid Interface Sci.*, 2014, **208**, 47–57.
41 S. Steltenkamp, M. M. Müller, M. Deserno, C. Hennesthal, C. Steinem and A. Janshoff, *Biophys. J.*, 2006, **91**, 217–226.
42 F. Olson, C. a. Hunt, F. C. Szoka, W. J. Vail and D. Papahadjopoulos, *Biochim. Biophys. Acta*, 1979, **557**, 9–23.
43 R. M. Dougherty, C. Galli, A. Ferro-Luzzi and J. M. Iacono, *Am. J. Clin. Nutr.*, 1987, **45**, 443–455.
44 H. Hagerstrand and B. Isomaa, *Biochim. Biophys. Acta, Biomembr.*, 1994, **1190**, 409–415.